Inorganic Chemistry

Article

pubs.acs.org/IC

Novel Ruthenium Sensitizers Having Different Numbers of Carboxyl Groups for Dye-Sensitized Solar Cells: Effects of the Adsorption Manner at the TiO_2 Surface on the Solar Cell Performance

Hironobu Ozawa, Takahito Sugiura, Ryosuke Shimizu, and Hironori Arakawa*

Department of Industrial Chemistry, Faculty of Engineering, Tokyo University of Science, 12-1, Ichigaya-Funagawara, Shinjuku, Tokyo 162-0826, Japan

Supporting Information

ABSTRACT: Two novel ruthenium sensitizers having multiple carboxyl groups ((TBA)[Ru{4′-(3,4-dicarboxyphenyl)-4,4″-dicarboxyterpyridine}$(NCS)_3$] (**TUS-21**) and (TBA)[Ru{4′-(3-carboxyphenyl)-4,4″-dicarboxyterpyridine}$(NCS)_3$] (**TUS-37**); TBA = tetrabutylammonium) have been synthesized as improved model sensitizers for the previously reported ruthenium sensitizer **TUS-20** ((TBA)[Ru{4′-(3,4-dicarboxyphenyl)terpyridine}$(NCS)_3$]). The absorption maxima of two MLCT bands and the absorption onsets of **TUS-21** and **TUS-37** were shifted to longer wavelengths of about 30 nm in comparison to those of **TUS-20** by introducing a carboxyl group to the each terminal pyridine ring of the terpyridine ligand. **TUS-21** and **TUS-37** showed quite similar adsorption behaviors to the TiO_2 surface, and this adsorption behavior was found to be different from that of **TUS-20**. ATR-IR measurements revealed that **TUS-21** and **TUS-37** bind to the TiO_2 surface by using two carboxyl groups at the 3-position of the phenyl ring and at one of the terminal pyridine rings of the terpyridine ligand, while **TUS-20** is reported to bind by using two carboxyl groups at the 3,4-dicarboxyphenyl unit. The dye-sensitized solar cell (DSC) with **TUS-21** exhibited 10.2% conversion efficiency, which is much higher than that of the DSC with **TUS-20** (7.5%), under AM 1.5 (100 mW/cm^2) irradiation.

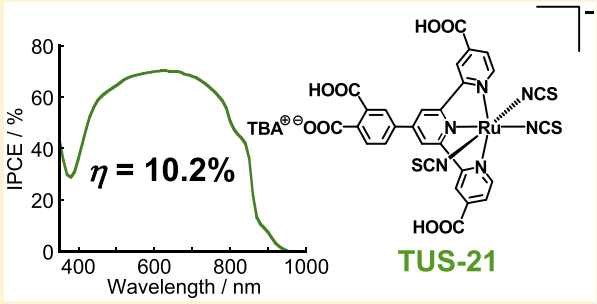

INTRODUCTION

Solar energy conversion has attracted significant attention because solar light is a clean and abundant energy. In this regard, extensive efforts have been devoted to develop photovoltaic devices which can perform highly efficient solar-to-electrical energy conversion for the effective utilization of the solar energy. Dye-sensitized solar cells (DSCs) are considered to be one of the most promising next-generation photovoltaic devices due to the relatively higher light-to-electrical energy conversion efficiency with a lower production cost.[1] The conversion efficiency of the DSC has increased gradually by developing efficient sensitizers, TiO_2 photoelectrodes, and counter electrodes and by optimizing the electrolyte composition. Recently, the conversion efficiency of the DSCs has exceeded 13% by using traditional molecular sensitizers, such as Zn porphyrin sensitizers.[2] In addition, around 15% conversion efficiency has been achieved in the perovskite-based DSCs.[3] These perovskite-based DSCs exhibit extremely higher conversion efficiency; however, perovskite sensitizers employed in these studies cannot utilize near-IR light (λ >800 nm) effectively. Therefore, the obtained photocurrent density values (J_{sc}) in these highly efficient perovskite-based DSCs are not as high (around 21 mA/cm^2). For comparison, several highly efficient ruthenium sensitizers can utilize near-IR light (800−950 nm) more effectively as well as visible light. However, the J_{sc} values obtained in the DSCs with these highly efficient ruthenium sensitizers were almost the same (J_{sc} > 21 mA/cm^2)[4] as those of highly efficient perovskite-based DSCs due to the relatively smaller molar absorptivity of ruthenium sensitizers. One of the most famous and highly efficient ruthenium sensitizers is black dye[5] ($(TBA)_3$[Ru(Htcterpy)$(NCS)_3$]; TBA = tetrabutylammonium, tcterpy = 4,4′,4″-tricarboxy-2,2′:6′,2″-terpyridine; Figure 1). To date, conversion efficiency higher than 10.5% has been obtained in DSCs with black dye,[6] and conversion efficiency higher than 11% has been achieved in a cosensitized DSC with black dye and an organic dye.[7] In order to take advantage of the superior absorption properties of these ruthenium sensitizers in the near-IR region, one of the most important points for further improvement of the conversion efficiency of DSCs is to increase the molar absorptivity of the ruthenium sensitizers, because the absorption coefficient of ruthenium sensitizers is 1 order of magnitude smaller than that of perovskite sensitizers.[2c,8] In this context, a large number of ruthenium sensitizers having a chromophore unit, such as a thienyl, stylenyl, triphenylamine, or carbazole derivative, at the bipyridine or the terpyridine ligand have thus far been synthesized.[9] These ruthenium sensitizers actually have a strong absorption band corresponding to the $\pi-\pi^*$ transition of the chromophore unit at the visible region (350−600 nm);

Received: June 20, 2014
Published: August 21, 2014

   dx.doi.org/10.1021/ic501479p | Inorg. Chem. 2014, 53, 9375−9384

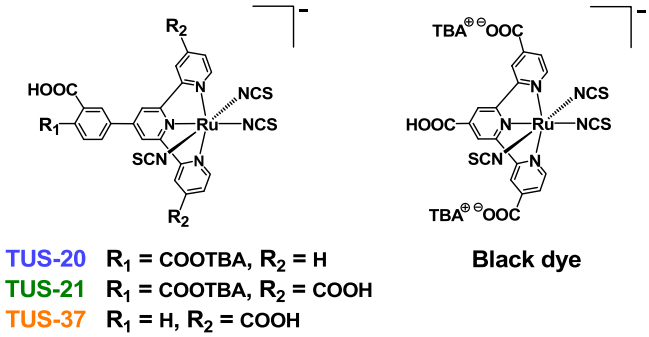

Figure 1. Structures of **TUS-20**, **TUS-21**, **TUS-37**, and black dye.

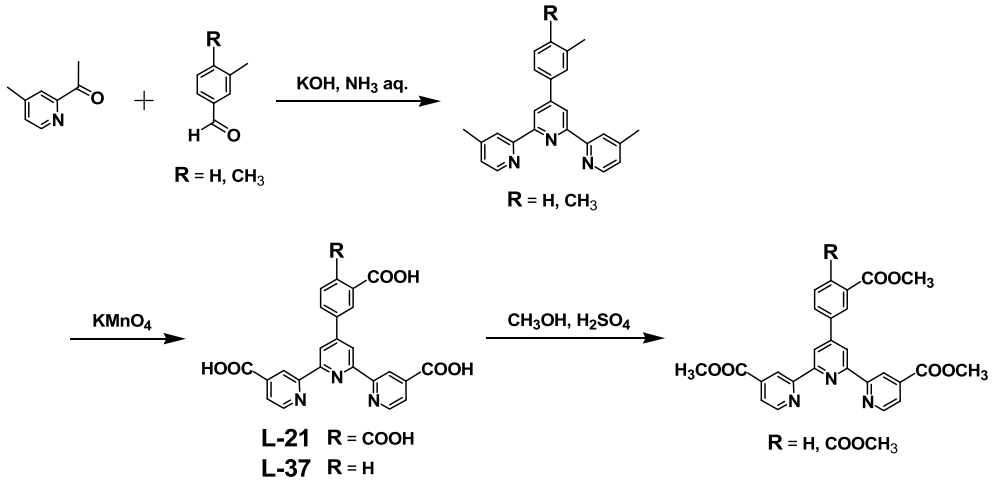

Figure 2. Synthetic scheme of the two novel ligands **L-21** and **L-37**.

however, molar absorptivity at the MLCT band extending into the near-IR region is not increased effectively by these structural modifications. Therefore, the incident photon-to-current conversion efficiency (IPCE) of the DSCs in the near-IR region is not improved effectively by these structural modifications. These studies seem to suggest that improvement of the molar absorptivity at the MLCT band is essential for further efficiency improvement of the DSCs with ruthenium sensitizers.

On the other hand, continuous efforts have been devoted in our group to develop ruthenium sensitizers showing a conversion efficiency higher than that of black dye. We reported recently that the molar absorptivity of the ruthenium sensitizer **TUS-20** (Figure 1), which possesses a 3,4-dicarboxyphenyl group as an anchor unit, at the MLCT band, is larger than that of black dye, even though **TUS-20** does not have a chromophore unit. However, the conversion efficiency of a DSC with **TUS-20** (7.3%) is found to be lower than that obtained in a DSC with black dye (10.4%).[10] The reason for this lower performance of **TUS-20** is reported to be both the lower IPCE values of the DSC in the wavelength range beyond 650 nm and the promoted backward electron transfer reaction from the conduction band of TiO_2 to the oxidized form of the dye and/or to I_3^- in the electrolyte solution.[10] In this study, two novel ruthenium sensitizers (**TUS-21** and **TUS-37**; Figure 1) have been synthesized as improved model sensitizers for **TUS-20**. By introduction of a carboxyl group to each terminal pyridine ring of the terpyridine ligand, the absorption maxima of two MLCT bands and the absorption onsets of these two ruthenium sensitizers are expected to shift to the longer wavelength region without a decrease in the molar absorptivity. Such red shifts of the absorption maxima and the absorption onsets would improve the IPCE values of the DSCs at the wavelength range above 650 nm. Here we report syntheses, photo- and electrochemical properties, and solar cell performances of DSCs with **TUS-21** and **TUS-37**. Moreover, the effects of the number and the position of the carboxyl anchor group on the adsorption behavior of the ruthenium sensitizer to the TiO_2 surface and on the solar cell performances of the DSCs will also be reported.

RESULTS AND DISCUSSION

Synthesis. Two novel terpyridine ligands (**L-21** and **L-37**) were synthesized via the so-called Kröhnke reaction and then oxidation of the corresponding tetra- or trimethyl compound by $KMnO_4$ (Figure 2). Since the solubilities of **L-21** and **L-37** were quite low in conventional organic solvents, their purification and characterization were carried out after esterification of all the carboxyl groups by methanol. Partially oxidized species (byproducts) could be removed successfully after esterification, and fully oxidized species (target compounds) were characterized by ^1H NMR spectra. Each esterified compound was reacted with $RuCl_3 \cdot 3H_2O$ and further reacted with KNCS in DMF. The crude products were purified on a silica gel column several times using a mixed solvent of CH_3CN, saturated aqueous KNO_3, and H_2O as eluent and then further purified on a Sephadex LH-20 column using a TBAOH solution. Pure compounds of **TUS-21** and **TUS-37** were obtained as TBA salts with low synthetic yields (about 3%). Both ruthenium sensitizers were characterized successfully by

dx.doi.org/10.1021/ic501479p | Inorg. Chem. 2014, 53, 9375−9384

^{1}H NMR spectra, ESI-TOF MS, and elemental analysis. The amount of TBA^+ contained in **TUS-21** was estimated to be 2.0 from the ^{1}H NMR spectrum and elemental analysis. Since one of the TBA^+ exists as a countercation of **TUS-21**, the other TBA^+ would be present instead of one of the protons of the four carboxyl groups. From the ^{1}H NMR spectra, the proton of the carboxyl group at the 4-position of the phenyl ring is considered to be replaced by TBA^+. In the case of **TUS-37**, the amount of TBA^+ was estimated to be 1.25. From the ^{1}H NMR spectra, the proton of the carboxyl group at the 3-position of the phenyl ring is considered to be replaced partially by TBA^+. On the other hand, the amount of TBA^+ contained in **TUS-20** is reported to be 2.0, and one of the TBA^+ groups is considered to exist instead of the proton of the carboxyl group at the 4-position of the phenyl ring.[10b]

Photo- and Electrochemical Studies. Molar absorptivity spectra of **TUS-21**, **TUS-37**, and **TUS-20** together with that of black dye in DMF are shown in Figure 3. **TUS-21** and **TUS-37**

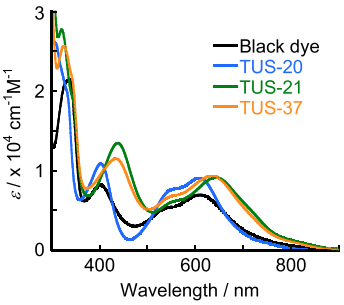

Figure 3. Molar absorptivity spectra of **TUS-20**, **TUS-21**, **TUS-37**, and black dye in DMF.

displayed quite similar absorption spectra, although molar absorptivity at the higher energy MLCT band (440 nm) of **TUS-21** was slightly larger than that of **TUS-37**. This result indicates that the presence of the carboxyl group at the 4-position of the phenyl ring does not affect the lower energy MLCT process at all. As is described below, lower energy LUMOs (LUMO and LUMO+1) of **TUS-21** and **TUS-37** were found to be located only at the terpyridine units. Therefore, the absorption maxima and molar absorptivities of the lower energy MLCT bands of **TUS-21** and **TUS-37** are almost equal, even though **TUS-37** does not possess a carboxyl group at the 4-position of the phenyl ring. On the other hand, the absorption maxima of the two MLCT bands and the absorption onsets of **TUS-21** and **TUS-37** shifted about 30 nm to longer wavelength in comparison to those of **TUS-20**. These red shifts of the absorption maxima of the lower energy MLCT bands and the absorption onsets clearly indicate that the energy gaps between the HOMO and LUMO of **TUS-21** and **TUS-37** are diminished by introducing the carboxyl group to the each terminal pyridine ring of the terpyridine ligand, which is mainly due to the stabilization of the π^* orbitals of the terpyridine ligand because π^* orbitals of the terpyridine ligands of **TUS-21** and **TUS-37** correspond to the LUMO and LUMO+1 as mentioned below. Since the molar absorptivities of two MLCT bands of **TUS-21** and **TUS-37** were almost equal to that of **TUS-20**, it is expected that DSCs with these two ruthenium sensitizers would show higher IPCE values at a wavelength range above 650 nm and exhibit J_{sc} values larger than that of the DSC with **TUS-20**.

On the other hand, phosphorescence from the ^{3}MLCT excited states of **TUS-21** and **TUS-37** could not be observed at room temperature, while that from **TUS-20** was observed centered at around 830 nm under the same conditions.[10b] Therefore, the quantum yield of the phosphorescence might be lowered by introducing a carboxyl group at the terminal pyridine ring of the terpyridine ligand. The lowest transition energies (E_{0-0}) of **TUS-21** and **TUS-37** were estimated from the onset wavelength of the absorption spectra.

Energy levels of the HOMOs of **TUS-21** and **TUS-37** were determined by cyclic voltammetry in DMF. Quasi-reversible oxidation waves, which are assignable to the Ru(II)/Ru(III) oxidation, were observed in **TUS-21** and **TUS-37** at 0.68 and 0.65 V vs SCE, respectively (Table 1). These values are almost

Table 1. Electrochemical Properties of TUS-21, TUS-37, TUS-20, and Black Dye[a]

sensitizer	E_{HOMO} (V vs SCE)	E_{0-0} (V)	E_{LUMO}[d] (V vs SCE)
TUS-21	0.68	1.61[b]	−0.93
TUS-37	0.65	1.58[b]	−0.93
TUS-20[c]	0.55	1.71	−1.16
black dye[c]	0.66	1.61	−0.95

[a]All potentials are given vs SCE. Oxidation potentials of **TUS-21** and **TUS-37** were measured in DMF containing 0.1 M $LiClO_4$. [b]E_{0-0} was estimated from the onset wavelength of the absorption spectrum. [c]Data from ref 10. [d]$E_{LUMO} = E_{HOMO} - E_{0-0}$.

equal to that of black dye and are about 0.1 V lower than that of **TUS-20**, which indicates that introduction of a carboxyl group to each terminal pyridine ring of the terpyridine ligand effectively lowered the energy levels of the HOMOs. On the other hand, the estimated energy level of LUMOs of both **TUS-21** and **TUS-37** was −0.93 V vs SCE, which is almost equal to that of black dye. These results indicate that presence of a carboxyl group at the 4-position of the phenyl ring does not affect the energy levels of HOMO and LUMO at all and that the energy levels of HOMOs and LUMOs of **TUS-21** and **TUS-37** are suitable for both effective electron injection from the excited states of dyes into the conduction band of TiO_2 and effective reduction of the resulting oxidized forms of dyes by I^- in the electrolyte solution.

DFT Calculations. Frontier molecular orbitals and the energy diagrams of **TUS-21** and **TUS-37** are shown in Figure 4 and Figure S1 (Supporting Information), respectively. In each sensitizer, HOMO and HOMO-1 are located mainly at the Ru(II) atom and two axial NCS ligands. LUMO and LUMO+1 are delocalized mainly over the terpyridine ligand. In addition, no remarkable difference was observed in the energy levels of these molecular orbitals between two sensitizers (Figure S1). Therefore, these results seem to agree with the fact that the absorption maxima and the molar absorptivities of the lower energy MLCT bands of **TUS-21** and **TUS-37** were almost equal, as mentioned above. On the other hand, LUMO+2 of **TUS-21**, which was stabilized in comparison to that of **TUS-37**, was populated mainly at the phenyl ring and LUMO+3 was delocalized over the terpyridine ligand. For comparison, LUMO+2 of **TUS-37** was delocalized over the terpyridine ligand, and LUMO+3 was populated mainly at both the phenyl ring and the central pyridine ring of the terpyridine ligand. This difference would be derived from the presence of the carboxyl group at the 4-position of the phenyl ring. In the case of **TUS-20**, which does not have the carboxyl group at each terminal

dx.doi.org/10.1021/ic501479p | Inorg. Chem. 2014, 53, 9375−9384

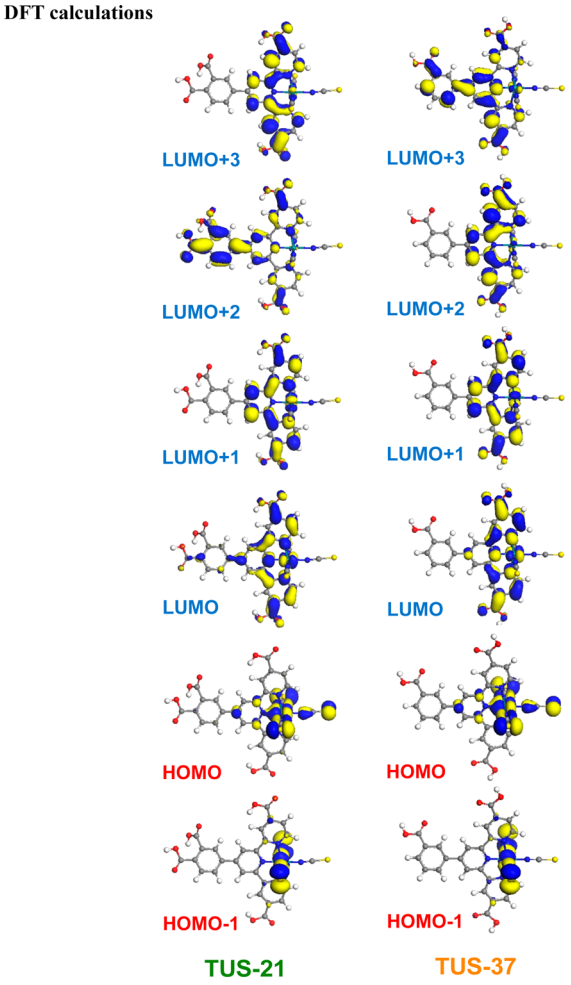

Figure 4. Frontier molecular orbitals of fully optimized structures of **TUS-21** and **TUS-37** in acetonitrile.

pyridine ring of the terpyridine ligand, the LUMO was populated at both the phenyl ring and the central pyridine ring of the terpyridine ligand.[10] LUMO+1 was delocalized over the terpyridine ligand.[10] In addition, **TUS-20** is reported to bind to the TiO_2 surface by using the 3,4-dicarboxyphenyl unit.[10] Consequently, the electron transfer reaction from the terpyridine ligand to the phenyl ring, which leads to electron injection into the TiO_2 group, is thermodynamically favorable.[10] If **TUS-21** binds to the TiO_2 surface by using the 3,4-dicarboxyphenyl unit just like **TUS-20**, effective electron injection into the TiO_2 is not expected because this electron transfer reaction from the terpyridine ligand to the phenyl ring is thermodynamically unfavorable. Therefore, the conversion efficiency of the DSC with **TUS-21** might be lower in such a case. In contrast, if **TUS-21** binds to the TiO_2 surface by using one of the carboxyl groups at the terminal pyridine rings of the terpyridine ligand, effective electron injection would occur because LUMO and LUMO+1 are delocalized at the terpyridine ligand. In the case of **TUS-37**, effective electron injection is not expected if **TUS-37** binds to the TiO_2 surface by using only the carboxyl group at the 3-position of the phenyl ring, because this electron transfer reaction is an uphill one. Further discussions about the effects of the binding manners of these ruthenium sensitizers at the TiO_2 surface on the solar cell performances of the DSCs will be carried out in the following section.

Adsorption Behavior of Dyes. We reported recently that **TUS-20** shows a superior adsorptivity to the TiO_2 surface.[10] For example, the adsorption rate is faster and the maximum amount of dye adsorption is greater in comparison to those of black dye and (TBA)[Ru(4′-carboxyterpydine)$(NCS)_3$], which is a structural analogue of **TUS-20**. Moreover, some amount of adsorbed **TUS-20** could not be desorbed from the TiO_2 photoelectrode by immersing the **TUS-20**-adsorbed TiO_2 photoelectrode into the NaOH solution for 1 day, while all adsorbed black dye and (TBA)[Ru(4′-carboxyterpydine)-$(NCS)_3$] could be desorbed easily and quickly (within a few minutes) by the same treatment.[10] This superior adsorptivity of **TUS-20** is considered to be due to the presence of the 3,4-dicarboxyphenyl group as an anchor unit.[11] It is also reported that both of the carboxyl groups of the 3,4-dicarboxyphenyl unit of **TUS-20** bind to the TiO_2 surface with a bidentate bridge mode (Figure 5).[10b] Since **TUS-21** also possesses the

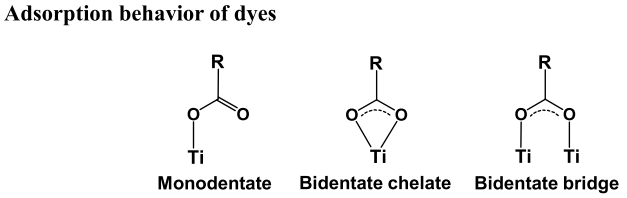

Figure 5. Possible binding modes of the carboxylate anchoring unit at the TiO_2 surface.

3,4-dicarboxyphenyl unit, it is expected that **TUS-21** shows a superior adsorptivity to the TiO_2 surface just like **TUS-20**. In addition, in order to know the effects of introduction of the carboxyl group at each terminal pyridine ring of the terpyridine ligand on the adsorption behavior, the adsorption behavior of **TUS-21** and **TUS-37** has been investigated. Figure 6 shows the

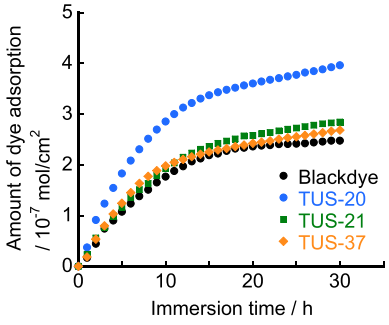

Figure 6. Adsorption profiles of **TUS-20**, **TUS-21**, **TUS-37**, and black dye to the TiO_2 photoelectrodes at 20 °C.

adsorption profiles of **TUS-20**, **TUS-21**, **TUS-37**, and black dye to the TiO_2 photoelectrode. As reported previously, the adsorption rate of **TUS-20** was actually faster and the maximum amount of dye adsorption of **TUS-20** was greater in comparison to those of black dye. On the other hand, the adsorption rate of **TUS-21** was slower and the maximum amount of dye adsorption was smaller in comparison to those of **TUS-20**. In addition, all adsorbed **TUS-21** could be desorbed from the TiO_2 photoelectrode easily and quickly by immersing into the NaOH solution. These results clearly indicate that **TUS-21** does not have a superior adsorptivity, even though **TUS-21** also possesses the 3,4-dicarboxyphenyl unit. In other words, these results suggest that **TUS-21** does

dx.doi.org/10.1021/ic501479p | Inorg. Chem. 2014, 53, 9375−9384

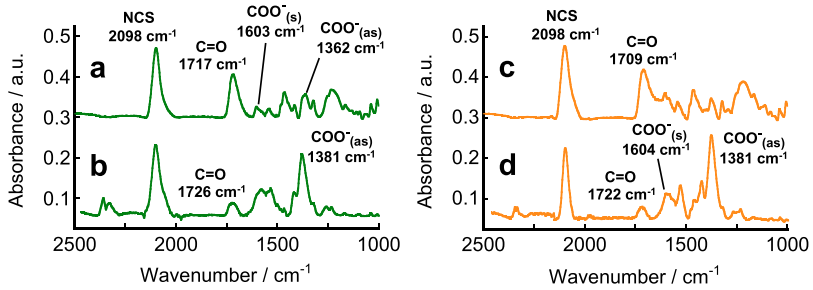

Figure 7. ATR-IR spectra of the powder sample of **TUS-21** (a), **TUS-21** adsorbed on TiO_2 nanoparticles (b), powder sample of **TUS-37** (c), and **TUS-37** adsorbed on TiO_2 nanoparticles (d).

not bind to the TiO_2 surface by using the 3,4-dicarboxyphenyl unit. In the case of **TUS-37**, the adsorption profile was quite similar to that of **TUS-21**, and all adsorbed **TUS-37** could be desorbed easily. These results imply that the adsorption manners of **TUS-21** and **TUS-37** at the TiO_2 surface are the same, that is to say, the carboxyl group at the 4-position of the phenyl ring of **TUS-21** does not participate in the binding to the TiO_2 surface.

In order to clarify the binding manners of **TUS-21** and **TUS-37** at the TiO_2 surface, ATR-IR measurements of these sensitizers before and after adsorption to the TiO_2 surface were conducted. The powder sample of **TUS-21** showed a strong absorption at 2098 cm^{-1} (Figure 7a), which is assigned to the stretching vibration mode of C═N of the N-bonded NCS ligands.[12] The relatively strong absorption band at 1717 cm^{-1} corresponds to the stretching vibration mode of C═O. Two absorption bands at 1603 and 1362 cm^{-1} are attributed to the symmetric and asymmetric stretching vibration modes of COO^-, respectively. The presence of the three bands ν(C═O), $\nu_s(COO^-)$, and $\nu_{as}(COO^-)$ in the powder sample of **TUS-21** agrees well with the fact that the carboxyl group at the 4-position of the phenyl ring of **TUS-21** exists as COO^- (the proton is replaced by TBA^+), and the other three carboxyl groups exist as COOH, as mentioned above. After adsorption to the TiO_2 surface, the peak intensity of the band of ν(C═O) decreased to about one-third, and the peak intensity of the two bands of $\nu_s(COO^-)$ and $\nu_{as}(COO^-)$ increased more than twice (Figure 7b). This result suggests that two of the three carboxyl groups of **TUS-21** participate in the binding, and the other carboxyl group still exists as COOH after adsorption to the TiO_2 surface. As described in DFT Calculations, it is considered that **TUS-21** does not bind to the TiO_2 surface by using the 3,4-dicarboxyphenyl unit. Therefore, **TUS-21** seems to bind by using two carboxyl groups at the 3-position of the phenyl ring and at one of the terminal pyridine rings of the terpyridine ligand, as shown in Figure 8. In this case, the carboxyl group at the other terminal pyridine ring of the terpyridine ligand still exists as COOH after adsorption. On the other hand, the separation width between the $\nu_s(COO^-)$ and the $\nu_{as}(COO^-)$ bands is known to be one of the criteria for the binding mode of the carboxyl anchor unit at the TiO_2 surface.[12] For example, the binding mode of the carboxyl anchor group is considered to be monodentate (Figure 5) in the case where the separation width of the dye adsorbed on the TiO_2 surface is equal to or larger than that of the powder sample of the dye.[12] On the other hand, the binding mode is considered to be a bidentate chelate or a bidentate bridge (Figure 5) in the case that the separation width of the dye adsorbed on the TiO_2 surface is smaller than that of the powder sample of the dye.[12] However, a bidentate chelate is reported to be highly unstable, from the results of DFT calculations.[12c] Consequently, the binding mode of the carboxyl anchor group can be concluded to be a bidentate bridge when the separation width between the $\nu_s(COO^-)$ and $\nu_{as}(COO^-)$ bands of the dye adsorbed on the TiO_2 surface is smaller than that of the powder sample of the dye.[12] In the case of **TUS-21**, the $\nu_{as}(COO^-)$ band (1362 cm^{-1}) shifted to higher frequency (1381 cm^{-1}) upon adsorption to the TiO_2 surface. The separation width between the $\nu_s(COO^-)$ and $\nu_{as}(COO^-)$ bands in the **TUS-21** adsorbed on the TiO_2 surface (220 cm^{-1}) was smaller than that of the powder sample of **TUS-21** (241 cm^{-1}), suggesting that the binding mode of each carboxyl group is a bidentate bridge mode (Figure 5).[12]

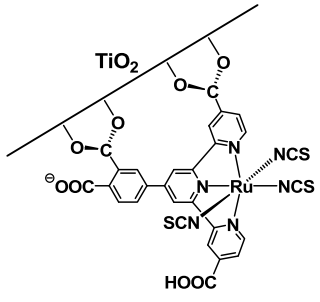

Figure 8. Speculated binding manner of **TUS-21** at the TiO_2 surface.

In the case of the powder sample of **TUS-37**, the strong absorption of ν(C═N) of the N-bonded NCS ligand and the relatively strong absorption of ν(C═O) were observed at 2098 and 1709 cm^{-1}, respectively (Figure 7c). Two characteristic bands corresponding to $\nu_s(COO^-)$ and $\nu_{as}(COO^-)$ were not observed, indicating that all three carboxyl groups of **TUS-37** exist as COOH. After adsorption to the TiO_2 surface, the peak intensity of the ν(C═O) band decreased to about one-third, and the two bands assignable to the $\nu_s(COO^-)$ and $\nu_{as}(COO^-)$ appeared at 1604 and 1381 cm^{-1}, respectively (Figure 7d). This result suggests that **TUS-37** binds to the TiO_2 surface by using the two carboxyl groups at the 3-position of the phenyl ring and at the terminal pyridine rings of the terpyridine ligand, just like **TUS-21**. The validity of these speculated binding manners of **TUS-21** and **TUS-37** is supported by the fact that the adsorption behaviors of **TUS-21** and **TUS-37** are quite similar to each other as described above.

By introducing the carboxyl group at the each terminal pyridine ring of the terpyridine ligand of **TUS-20**, the binding manner at the TiO_2 surface was changed. That is to say, **TUS-20** binds to the TiO_2 surface by using the 3,4-dicarboxyphenyl unit and **TUS-21** binds by using two carboxyl groups at the 3-position of the phenyl ring and at one of the terminal pyridine

dx.doi.org/10.1021/ic501479p | Inorg. Chem. 2014, 53, 9375−9384

rings of the terpyridine ligand, even though **TUS-21** also possesses the 3,4-dicarboxyphenyl unit. This difference in the binding manners between **TUS-20** and **TUS-21** seems to be derived from the difference in the reaction rates of bond formation between the carboxyl group and the OH group at the TiO_2 surface. Generally, the bond between the sensitizer and the TiO_2 surface is considered to form via a dehydration reaction of the COOH group of the sensitizer and the OH group at the TiO_2 surface. On the other hand, the bond between the COO^- group of the sensitizer and the OH group at the TiO_2 surface is considered to form through the substitution reaction of the OH group by the COO^- group. The reaction rate of the dehydration would be faster than that of the substitution reaction; therefore, the COOH group at the 3-position of the phenyl ring and one of the two COOH groups at the terminal pyridine rings of the terpyridine ligand participate dominantly in the binding to the TiO_2 surface in the case of **TUS-21**. As mentioned above, effective electron injection is not expected in **TUS-21** if **TUS-21** binds to the TiO_2 surface by using the 3,4-dicarboxyphenyl unit because the electron transfer from the terpyridine ligand to the phenyl ring, which leads to the electron injection into the TiO_2 group, is considered to be an uphill reaction. However, the obtained results suggest that effective electron injection into the TiO_2 group is possible in the cases of **TUS-21** and **TUS-37** because these two sensitizers bind to the TiO_2 surface by using one of the carboxyl groups at one of the terminal pyridine rings of the terpyridine ligand.

Solar Cell Performances of the DSCs. At first, solar cell performances of DSCs with **TUS-21** and **TUS-37** have been evaluated by using relatively thin TiO_2 photoelectrodes to investigate the effects of the presence of the carboxyl group at the 4-position of the phenyl ring. The DSC with **TUS-21** showed 8.6% conversion efficiency under this condition (Table 2). This efficiency is only slightly higher than that of **TUS-37**

Table 2. Solar Cell Performances of DSCs with TUS-21 and TUS-37[a]

sensitizer	J_{sc} (mA/cm^2)	V_{oc} (V)	FF	η (%)
TUS-21	19.03	0.632	0.711	8.55
TUS-37	19.14	0.630	0.690	8.32

[a]The electrolyte was an acetonitrile solution containing 0.05 M I_2, 0.1 M LiI, 0.6 M DMPImI, and 0.3 M TBP. The TiO_2 film thickness and active area were ca. 25 μm and 0.26 cm^2, respectively. Irradiation was carried out by using a solar simulator (AM 1.5, 100 mW/cm^2).

(8.3%); however, the obtained J_{sc} and V_{oc} values of the DSC with **TUS-21** were almost equal to those of the DSC with **TUS-37**. In addition, the shapes of the IPCE spectrum of each DSC were extremely similar to each other (Figure 9). These results indicate that presence of the carboxyl group at the 4-position of the phenyl ring has no effect not not only on photo- and electrochemical properties but also the solar cell performance. In addition, this result suggests that the binding manners of **TUS-21** and **TUS-37** at the TiO_2 surface are the same, although only **TUS-21** possesses the 3,4-dicarboxyphenyl unit. Further investigations have been carried out only for **TUS-21** by using our original thicker TiO_2 photoelectrode.[7c,d,g]

The DSC with **TUS-21** using our original thicker TiO_2 photoelectrode exhibited about 10% conversion efficiency, and 10.2% conversion efficiency was obtained in the DSC with an antireflection film and a black mask (Table 3). The obtained

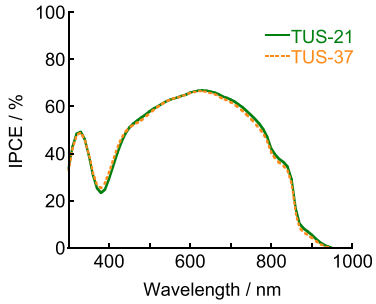

Figure 9. IPCE spectra of the DSCs with **TUS-21** and **TUS-37**.

Table 3. Solar Cell Performances of DSCs with TUS-20, TUS-21, and Black Dye[a]

sensitizer	J_{sc} (mA/cm^2)	V_{oc} (V)	FF	η (%)	amt of dye adsorption (10^{-7} mol/cm^2)
TUS-20	17.19	0.61	0.712	7.47	2.6[b]
TUS-21	20.83	0.68	0.704	9.97	2.1
TUS-21[c]	21.13	0.67	0.715	10.18	
black dye	21.61	0.70	0.716	10.81	2.3

[a]The electrolyte was an acetonitrile solution containing 0.05 M I_2, 0.1 M LiI, 0.6 M DMPImI, and 0.3 M TBP. The TiO_2 film thickness and active area were ca. 45 μm and 0.26 cm^2, respectively. Irradiation was carried out by using a solar simulator (AM 1.5, 100 mW/cm^2). [b]Some amount of adsorbed **TUS-20** could not be desorbed from the TiO_2 photoelectrode. [c]Solar cell performance of the DSC with an antireflection film and a black mask (0.221 cm^2).

conversion efficiency was much higher than that obtained in the DSC with **TUS-20** (7.5%), even though it was still slightly lower than that obtained in the DSC with black dye (10.8%). By introduction of the carboxyl group at each terminal pyridine ring of the terpyridine ligand, the conversion efficiency could be greatly increased. Both J_{sc} and V_{oc} values of the DSC with **TUS-21** were much larger than those of **TUS-20**. As shown in Figure 10, IPCE values of the DSC with **TUS-21** at the wavelength

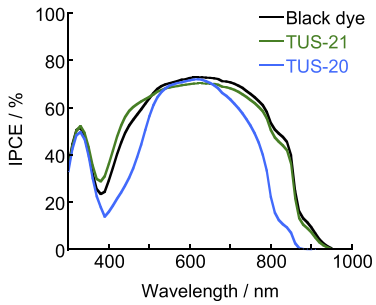

Figure 10. IPCE spectra of the DSCs with **TUS-20**, **TUS-21**, and black dye.

ranges between 380 and 520 nm and above 680 nm were much higher than those of **TUS-20**, even though the amount of dye adsorption of **TUS-21** was smaller (Table 3). These higher IPCE values could be attributed mainly to the relatively large red shift of the absorption maxima of two MLCT bands and the absorption onset of **TUS-21**, as mentioned above. In addition, the favorable binding manner of **TUS-21** at the TiO_2 surface might contribute to some extent to the obtained higher IPCE values. We reported recently that the electron injection reaction from the excited state of the dye into the conduction band of

dx.doi.org/10.1021/ic501479p | Inorg. Chem. 2014, 53, 9375−9384

TiO_2 occurs more effectively in the case where the path length of this electron transfer reaction is shorter.[10b] As described in the previous section, **TUS-21** is considered to bind to the TiO_2 surface by using two carboxyl groups at the 3-position of the phenyl ring and at the one of the terminal pyridine rings of the terpyridine ligand. In this case, one of the path lengths of the electron injection reaction is shorter (Figure 8) than that of **TUS-20** because **TUS-20** binds to the TiO_2 surface by using the 3,4-dicarboxyphenyl unit. On the other hand, this binding manner of **TUS-21** seems to improve not only the J_{sc} value but also the V_{oc} value. In the case of **TUS-20**, a relatively large vacancy exists at the **TUS-20**-adsorbed TiO_2 surface due to the presence of the phenyl ring, which might promote the access of I_3^- to the TiO_2 surface (Figure 11). In such a case, the

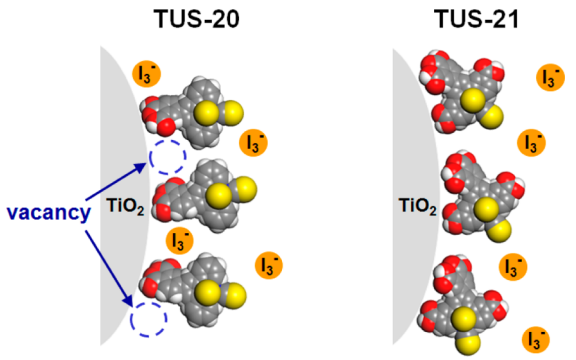

Figure 11. Speculated interfacial interaction between I_3^- and the TiO_2 surface.

backward electron transfer reaction from TiO_2 to I_3^- is enhanced, resulting in a decrease in the V_{oc} value. Actually, the backward electron transfer reaction is reported to be promoted in the DSC with **TUS-20**.[10] For comparison, such a vacancy does not exist at the **TUS-21**-adsorbed TiO_2 surface due to the different binding manner. Therefore, a relatively large V_{oc} value seems to be obtained in the DSC with **TUS-21**. Further investigations have been carried out to confirm the validity of this consideration.

Open-circuit voltage decay (OCVD) measurements for the DSCs with **TUS-20**, **TUS-21**, and black dye have been conducted to obtain insights into the backward electron transfer reactions from the conduction band of TiO_2. As shown in Figure 12, the electron lifetime in the TiO_2 photoelectrode of the DSC with **TUS-20** was much shorter than those of **TUS-21** and black dye at the matching V_{oc} value. This result suggests strongly that the backward electron transfer reaction is promoted greatly in the case of **TUS-20**. On the

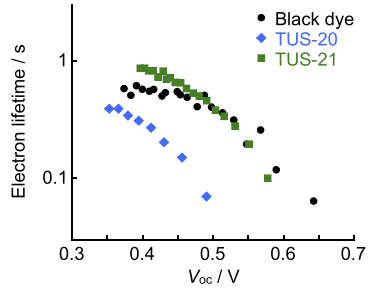

Figure 12. Electron lifetimes as a function of V_{oc} of the DSCs with **TUS-20**, **TUS-21**, and black dye.

other hand, this result also suggests that the backward electron transfer reaction is suppressed effectively in the case of **TUS-21**. This longer electron lifetime would be the other reason for the relatively large efficiency improvement in the DSC with **TUS-21**.

Electrochemical impedance spectroscopic (EIS) measurements under irradiation conditions have been carried out to obtain further insights into the internal resistances in the DSCs. As shown in Figure 13, R2 resistance, which corresponds

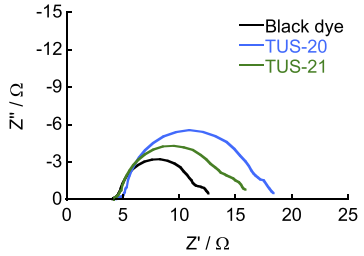

Figure 13. Electrochemical impedance spectra (Nyquist plots) of the DSCs with **TUS-20**, **TUS-21**, and black dye under AM 1.5 irradiation and open-circuit conditions.

mainly to the interfacial resistance at the TiO_2/dye/electrolyte interface, of the DSC with **TUS-20** was larger than those of black dye and **TUS-21**. This result also indicates that the backward electron transfer reaction from the TiO_2 to the oxidized form of the dye and/or to I_3^- in the electrolyte solution is promoted in the case of **TUS-20**. On the other hand, R2 resistance of the DSC with **TUS-21** was found to be larger than that of black dye. This result suggests that the backward electron transfer reaction in the DSC with **TUS-21** is slightly enhanced in comparison to the DSC with black dye. This slightly enhanced backward electron transfer reaction seems to be a major reason for the slightly smaller V_{oc} value and relatively lower conversion efficiency of the DSC with **TUS-21** in comparison to those of the DSC with black dye.

CONCLUSIONS

Two novel ruthenium sensitizers having multiple carboxyl groups (**TUS-21** and **TUS-37**) have been synthesized as improved model sensitizers for the previously reported sensitizer **TUS-20**. By introduction of the carboxyl group at each terminal pyridine ring of the terpyridine ligand, the absorption maxima of two MLCT bands and the absorption onset shifted about 30 nm to longer wavelengths in comparison to those of **TUS-20**. On the other hand, **TUS-21** does not have a superior adsorptivity to the TiO_2 surface, even though **TUS-21** also possesses the 3,4-dicarboxyphenyl unit. ATR-IR measurements revealed that **TUS-21** binds to the TiO_2 surface by using not the 3,4-dicarboxyphenyl unit but the two carboxyl groups at the 3-position of the phenyl ring and at one of the terminal pyridine rings of the terpyridine ligand.

The DSCs with **TUS-21** and **TUS-37** showed almost the same performance, indicating that presence of the carboxyl group at the 4-position of the phenyl ring does not affect the solar cell performance of the ruthenium sensitizer at all. The DSC with **TUS-21** using a thick TiO_2 photoelectrode showed about 10% conversion efficiency, which is much higher than that of **TUS-20** (7.5%), although it is slightly lower than that with black dye (10.8%). The efficiency improvement of **TUS-21** can be attributed mainly to the relatively large red shifts of the absorption maxima of two MLCT bands and the absorption

dx.doi.org/10.1021/ic501479p | Inorg. Chem. 2014, 53, 9375−9384

onset by introduction of the carboxyl group at each terminal pyridine ring of the terpyridine ligand. In addition, the favorable adsorption manner of **TUS-21** at the TiO_2 surface is considered to contribute to the efficiency improvement to some extent because the path length of the electron injection reaction from the excited state of the dye into the conduction band of TiO_2 is shorter than that of **TUS-20**. The conversion efficiency could be improved effectively by introducing the carboxyl group at the each terminal pyridine ring of the terpyridine ligand, and 10.2% conversion efficiency was obtained in the DSC with **TUS-21** under AM 1.5 (100 mW/cm^2) irradiation. This study provides valuable information on the effects of the number and position of the carboxyl anchor groups of the ruthenium sensitizers on both the adsorption behavior to the TiO_2 surface and the solar cell performances of the DSCs.

EXPERIMENTAL SECTION

Materials and General Measurements. Black dye ($(TBA)_3$[Ru(Htcterpy)$(NCS)_3$])[5] and **TUS-20**[10a] were prepared according to the literature methods. Titanium tetraisopropoxide and deoxycholic acid (DCA) were purchased from Tokyo Chemical Industry Co. 1,2-Dimethyl-3-propylimidazolium iodide (DMPImI) was purchased from Shikoku Kasei. 4-*tert*-Butylpyridine (TBP) was purchased from Sigma-Aldrich. All solvents and reagents were of the highest quality available and were used as received.

The elemental analysis was carried out on a PerkinElmer 2400II elemental analyzer using acetanilide as a standard material. ^{1}H NMR spectra were acquired on a Bruker BioSpin AVANCE 400 M spectrometer, where chemical shifts in $CDCl_3$, CD_3CN, DMSO, and CD_3OD were referenced to internal standard tetramethylsilane. ESI-TOF (electrospray ionization time-of-flight) mass spectra were recorded on a Bruker Micromass focus spectrometer. UV−visible absorption spectra were recorded on a Shimadzu UV-2550 spectrophotometer. Electrochemical measurements were carried out in DMF at a sweep rate of 50 mV/s using a glassy-carbon-disk working electrode, a Pt-wire counter electrode, and a Ag-wire reference electrode (ca. 330 mV vs SCE). The supporting electrolyte was 0.1 M $TBAClO_4$. ATR-IR spectra were recorded on a Shimadzu IRPrestige-21 spectrometer equipped with a single-reflection ATR accessory (MIRacle with a diamond prism plate).

DFT Calculations. MO calculations were carried out using the DFT methods implemented in the DMol^3 code package in Materials Studio 5.5 (Accelrys Inc.). Ground-state geometry optimization was performed using the generalized gradient corrected (GGA) function by Perdew, Barke, and Ernzerhof (PBE). Calculations were performed using the double numerical plus polarization (DNP) basis set. The core electrons were treated with DFT semicore pseudopotentials (DSPPs).

Synthesis. *4′-(3,4-Dimethylphenyl)-4,4″-dimethylterpyridine.* 2-Acetyl-4-methylpyridine (7.5 mmol, 1.0 g) and 3,4-dimethylbenzaldehyde (3.8 mmol, 0.5 mL) were dissolved in 40 mL of ethanol. KOH (10 mmol, 0.57 g) was dissolved in 23 mL of NH_3(aq) (30%), and this solvent was added to the former solution. This mixture was stirred for 1 day at 60 °C. The white precipitate was filtrated, washed with a mixed solvent of ethanol and water (4/1, v/v), and dried in vacuo; yield 0.62 g (1.7 mmol, 45%). ^{1}H NMR (400 MHz, $CDCl_3$): δ 8.69 (s, 2H), 8.59 (d, J = 5.0 Hz, 2H), 8.47 (s, 2H), 7.70 (s, 1H), 7.66 (d, J = 7.8 Hz, 1H), 7.26−7.25 (m, 1H), 7.17 (d, J = 4.8 Hz, 2H), 2.52 (s, 6H), 2.37 (s, 3H), 2.33 (s, 3H).

*4′-(3,4-Dicarboxyphenyl)-4,4″-dicarboxyterpyridine (**L-21**).* 4′-(3,4-Dimethylphenyl)-4,4″-dimethylterpyridine (5 mmol, 1.83 g) was dissolved in 50 mL of pyridine. $KMnO_4$ (75 mmol, 11.9 g) was suspended in 50 mL of H_2O, and this mixture was added to the former solution. This mixture was stirred for 2 h at 90 °C. Further $KMnO_4$ (75 mmol, 11.9 g) was added to the reaction mixture, which was then stirred for 2 h at 90 °C. This procedure was repeated twice, and then the reaction mixture was stirred overnight at 90 °C. MnO_2 was filtered and washed with a large amount of H_2O. Each filtrate was mixed and evaporated to dryness. The residue was dissolved in H_2O, and then concentrated HCl was added until a white precipitate formed (pH 1.0). This white precipitate was filtered, washed with water, and dried in vacuo; yield 1.73 g (3.8 mmol, 71%). Purification of this compound was difficult due to its low solubility in common organic solvents; therefore, purification was not carried out at this step.

4′-(3,4-Dimethoxycarbonylphenyl)-4,4″-dimethoxycarbonylterpyridine. **L-21** (1 mmol, 0.49 g) was suspended in 45 mL of CH_3OH, and then 5 mL of H_2SO_4 was added to this solution. This mixture was refluxed for 1 day under N_2. A 90 mL portion of H_2O was added, and then NH_3(aq) was added to adjust the pH to 2.5. The white precipitate was filtered, washed with CH_3OH, and dried in vacuo; yield 0.32 g (0.6 mmol, 60%). ^{1}H NMR (400 MHz, DMSO): δ 8.99−8.97 (m, 4H), 8.77 (s, 2H), 8.23−8.22 (m, 2H), 7.98−7.94 (m, 3H), 4.00 (s, 6H), 3.90 (s, 3H), 3.89 (s, 3H).

Ru(4′-(3,4-dimethoxycarbonylphenyl)-4,4″-dimethoxycarbonylterpyridine)Cl$_3$. $RuCl_3 \cdot 3H_2O$ (3.26 mmol, 0.86 g) and 4′-(3,4-dimethoxycarbonylphenyl)-4,4″-dimethoxycarbonylterpyridine (2.51 mmol, 1.36 g) were dissolved in 200 mL of a mixed solvent of C_2H_5OH and chloroform (3/1, v/v). This mixture was refluxed for 5 h and and then condensed to ca. 30 mL. The dark brown precipitate was filtered, washed with C_2H_5OH, and dried in vacuo; yield 1.89 g (2.5 mmol, quantitative). Characterization could not be carried out due to the low solubility of this compound.

*(TBA)[Ru(**L-21**)(NCS)$_3$]·TBA·3H$_2$O (**TUS-21**).* Ru(4′-(3,4-dimethoxycarbonylphenyl)-4,4″-dimethoxycarbonylterpyridine)Cl_3 (2.87 mmol, 2.15 g) and TBANCS (43 mmol, 12.9 g) were dissolved in 200 mL of a mixed solvent of DMF and H_2O (3/1, v/v). $N(C_2H_5)_3$ (215 mmol, 21.8 g) was added to this solution, which was then refluxed for 62 h under N_2 in the dark. The reaction mixture was evaporated to dryness, and the residue was dissolved in 0.1 M TBAOH solution. HCl (0.5 M) was added until a precipitate formed (around pH 3.0). This precipitate was filtered and washed with H_2O. Purification was carried out on a silica gel column using a mixed solvent of CH_3CN, saturated KNO_3, and H_2O (14/1/2, v/v) several times. The dark green band was collected and evaporated to dryness. The residue was dissolved in 0.1 M TBAOH solution. HCl (0.5 M) was added until a dark green precipitate formed. This dark green powder was further purified by a Sephadex LH-20 column using TBAOH solution as an eluent several times. The dark blue band was collected, and 0.5 M HCl was added until a dark green precipitate formed.The dark green precipitate was filtered, washed with H_2O, and dried in vacuo; yield 0.1 g (0.08 mmol, 3.5%). ^{1}H NMR (400 MHz, CD_3CN): δ 9.14 (d, J = 6.0 Hz, 2H), 8.95 (s, 2H), 8.85 (s, 1H), 8.79 (s, 2H), 8.37 (d, J = 8.5 Hz, 1H), 8.24 (d, J = 9.5 Hz, 1H), 8.14 (d, J = 6.5 Hz, 1H), 3.13−3.07 (m, 16H), 1.66−1.58 (m, 16H), 1.42−1.33 (m, 16H), 1.00−0.97 (m, 24H). Anal. Calcd for ([**M**]·2TBA·3H$_2$O): C, 55.49; H, 7.14; N, 8.63. Found: C, 55.76; H, 6.90; N, 8.82.

4′-(3-Methylphenyl)-4,4″-dimethylterpyridine. 2-Acetyl-4-methylpyridine (30 mmol, 3.9 g) and *m*-tolualdehyde (15 mmol, 1.8 mL) were dissolved in 150 mL of ethanol. KOH (40 mmol, 2.2 g) was dissolved in 90 mL of NH_3(aq) (30%), and this solvent was added to the former solution. This mixture was stirred for 1 day at 60 °C. The white precipitate was filtered, washed with a mixed solvent of ethanol and water (4/1, v/v), and dried in vacuo; yield 2.67 g (51%). ^{1}H NMR (400 MHz, DMSO): δ 8.70 (s, 2H), 8.61 (d, J = 5.0 Hz, 2H), 8.51 (s, 2H), 7.73 (s, 1H), 7.70 (d, J = 8.0 Hz, 1H), 7.49 (t, J = 7.5 Hz, 1H), 7.37−7.35 (m, 3H), 2.52 (s, 6H), 2.46 (s, 3H).

*4′-(3-Carboxyphenyl)-4,4″-dicarboxyterpyridine (**L-37**).* 4′-(3-Methylphenyl)-4,4″-dimethylterpyridine (4.8 mmol, 1.7 g) was dissolved in 50 mL of pyridine. $KMnO_4$ (75 mmol, 11.9 g) was suspended in 50 mL of H_2O, and this mixture was added to the former solution. This mixture was stirred for 2 h at 90 °C. Further $KMnO_4$ (75 mmol, 11.9 g) was added to the reaction mixture, which was then stirred for 2 h at 90 °C. This procedure was repeated twice, and then the reaction mixture was stirred overnight at 90 °C. MnO_2 was filtered and washed with a large amount of H_2O. Each filtrate was mixed and evaporated to dryness. The residue was once dissolved in H_2O, and then concentrated HCl was added until a white precipitate formed (pH 1.0). This white precipitate was filtered, washed with water, and

dx.doi.org/10.1021/ic501479p | Inorg. Chem. 2014, 53, 9375−9384

dried in vacuo; yield 1.88 g (88%). Purification of this compound was difficult due to its low solubility in common organic solvents; therefore, purification was not carried out at this step.

4′-(3-Methoxycarbonylphenyl)-4,4″-dimethoxycarbonylterpyridine. **L-37** (7.7 mmol, 3.7 g) was suspended in 400 mL of CH_3OH, and then 30 mL of H_2SO_4 was added to this solution. This mixture was refluxed for 1 day under N_2. A 600 mL portion of H_2O was added, and then NH_3(aq) was added to adjust the pH to 2.5. The white precipitate was filtered, washed with CH_3OH, and dried in vacuo; yield 2.5 g (69%). ^{1}H NMR (400 MHz, CD_3CN)): δ 9.49 (d, J = 6.0 Hz, 2H), 9.40 (s, 2H), 9.01 (s, 2H), 8.73 (s, 1H), 8.63 (d, J = 5.5 Hz, 2H), 8.33 (d, J = 8.0 Hz, 1H), 8.29 (d, J = 8.0 Hz, 1H), 7.84 (t, J = 7.8 Hz, 1H), 4.13 (s, 6H), 4.01 (s, 3H).

Ru(4′-(3-methoxycarbonylphenyl)-4,4″-dimethoxycarbonylterpyridine)Cl$_3$. $RuCl_3{\cdot}3H_2O$ (6.87 mmol, 1.8 g) and 4′-(3-methoxycarbonylphenyl)-4,4″- dimethoxycarbonylterpyridine (5.28 mmol, 2.55 g) were dissolved in 380 mL of acetonitrile. This mixture was refluxed overnight and then condensed to ca. 30 mL. The dark brown precipitate was filtered, washed with C_2H_5OH, and dried in vacuo; yield 2.95 g (81%). Characterization could not be carried out due to the low solubility of this compound.

*(TBA)[Ru(**L-37**)(NCS)$_3$]·0.25TBA·3H$_2$O (**TUS-37**).* Ru(4′-(3-methoxycarbonylphenyl)-4,4″-dimethoxycarbonylterpyridine)Cl_3 (2.87 mmol, 2.95 g) and KNCS (51 mmol, 5.0 g) were dissolved in 300 mL of a mixed solvent of DMF and H_2O (2/1, v/v). $N(C_2H_5)_3$ (215 mmol, 21.8 g) was added to this solution, which was then refluxed for 62 h under N_2 in the dark. The reaction mixture was evaporated to dryness, and the residue was dissolved in 0.1 M TBAOH solution. HCl (0.5 M) was added until the precipitate formed (around pH 3.0). This precipitate was filtered and washed with H_2O. Purification was carried out on a silica gel column using a mixed solvent of CH_3CN, saturated KNO_3, and H_2O (14/1/2, v/v) several times. The dark green band was collected and evaporated to dryness. The residue was dissolved in 0.1 M TBAOH solution. HCl (0.5 M) was added until a dark green precipitate formed. This dark green powder was further purified by a Sephadex LH-20 column using TBAOH solution as an eluent several times. The dark blue band was collected, and 0.5 M HCl was added until a dark green precipitate formed. The dark green precipitate was filtered, washed with H_2O, and dried in vacuo; yield 0.11 g (2.3%). ^{1}H NMR (400 MHz, CD_3OD): δ 9.16 (m, 2H), 8.94 (s, 2H), 8.77 (s, 2H), 8.70 (s, 1H), 8.32 (d, J = 7.5 Hz, 1H), 8.16−8.15 (m, 3H), 7.72 (t, J = 7.8 Hz, 1H), 3.25−3.21 (m, 10H), 1.70−1.62 (m, 10H), 1.45−1.36 (m, 10H), 1.03−0.99 (m, 15H). ESI-TOF MS (negative ion, CH_3OH): 716.77 m/z ($[\mathbf{M}]^-$). Anal. Calcd for ($[\mathbf{M}]{\cdot}1.25TBA{\cdot}3H_2O$): C, 52.57; H, 6.19; N, 9.46. Found: C, 52.75; H, 6.41; N, 9.59.

Preparation of TiO$_2$ Electrode and DSC. TiO_2 pastes were prepared using titanium tetraisopropoxide.[5] Nanocrystalline TiO_2 photoelectrodes were prepared by screen printing the TiO_2 paste on fluorine-doped SnO_2 conducting glasses (FTO, Nippon Sheet Glass Co., 10 Ω/square). TiO_2 films were composed of seven layers (from the bottom to the third layer, 20 nm TiO_2 particles, fourth and fifth layers, a 8/2 mixture of 20 and 100 nm particles; sixth layer, a 6/4 mixture of 20 and 100 nm particles; top layer, 400 nm TiO_2 particles; film thickness, approximately 45 μm). TiO_2 photoelectrodes were calcinated at 520 °C after every layer was coated. The active areas of these TiO_2 photoelectrode were determined using a KEYENCE VHX-200 digital microscope. The TiO_2 photoelectrodes were immersed in a 1-propanol solution of 0.2 mM black dye and 20 mM DCA, an ethanol solution of 0.2 mM **TUS-20** and 20 mM DCA, a 1-propanol solution of 0.2 mM **TUS-21** and 20 mM DCA, or a 1-propanol solution of 0.2 mM **TUS-37** and 20 mM DCA for 22 h at room temperature to adsorb dyes onto the TiO_2 surface.

Photoelectrochemical measurements were performed in a two-electrode sandwich cell configuration made up of the dye-adsorbed TiO_2 electrode, a platinum-sputtered counter electrode, a spacer film (50 μm), and an electrolyte solution (0.05 M I_2, 0.1 M LiI, 0.6 M DMPImI, and 0.3 M TBP in acetonitrile). Black dye, **TUS-21**, and **TUS-37** were desorbed from the TiO_2 photoelectrode by immersing in 0.05 M NaOH solution, and the amount of dye adsorption was estimated from the absorption spectrum of the resulting solution. Some amount of **TUS-20** could not be desorbed from the TiO_2 photoelectrode by immersion more than 24 h.

The photocurrent−voltage (I−V) characteristics of the DSCs were measured on a Keithley 2400 source meter under irradiation of AM 1.5, 100 mW/cm^2 (1 sun), supplied by a solar simulator (Yamashita Denso, YSS-150A). The incident light intensity was calibrated with an LS-100 grating spectroradiometer (EKO Instruments) and Si photodiode (Bunkoh Keiki). The incident monochromatic photon-to-current conversion efficiency (IPCE) was measured on a PEC-S10 instrument (Peccell Technologies). Electrochemical impedance spectroscopic (EIS) studies were conducted using an SI 1287 electrochemical interface (Solartron) and a 1255B frequency response analyzer (Solartron).

■ ASSOCIATED CONTENT

Ⓢ Supporting Information

A figure giving energy diagrams of the fully optimized structures of **TUS-21** and **TUS-37** in acetonitrile. This material is available free of charge via the Internet at http://pubs.acs.org.

■ AUTHOR INFORMATION

Corresponding Author

*H.A.: e-mail, h.arakawa@ci.kagu.tus.ac.jp; fax, (+81) 3 5261 4631; tel, (+81) 3 5228 8311.

Notes

The authors declare no competing financial interest.

■ ACKNOWLEDGMENTS

This work was supported by the New Energy and Industrial Technology Development Organization (NEDO) of Japan. H.O. acknowledges a Grant-in-Aid for young scientist (B) (No. 25810043) from the Ministry of Education, Culture, Sports, Science, and Technology of Japan.

■ REFERENCES

(1) (a) O'Regan, B.; Grätzel, M. *Nature* **1991**, *353*, 737−740. (b) Nazeeruddin, M. K.; Kay, A.; Rodicio, I.; Humphry-Baker, R.; Müller, E.; Liska, P.; Vlachopoulos, N.; Grätzel, M. *J. Am. Chem. Soc.* **1993**, *115*, 6382−6390. (c) Grätzel, M. *Acc. Chem. Res.* **2009**, *42*, 1788−1798. (d) Hagfeldt, A.; Boschloo, G.; Sun, L.; Kloo, L.; Pettersson, H. *Chem. Rev.* **2010**, *110*, 6595−6663. (e) Yum, J.-H.; Baranoff, E.; Wenger, S.; Nazeeruddin, M. K.; Grätzel, M. *Energy. Environ. Sci.* **2011**, *4*, 842−857.

(2) (a) Yella, A.; Lee, H.-W.; Tsao, H. N.; Yi, C.; Chandiran, A. K.; Nazeeruddin, M. K.; Diau, E. W.-G.; Yeh, C.-Y.; Zakeeruddin, S. M.; Grätzel, M. *Science* **2011**, *334*, 629−634. (b) Mathew, S.; Yella, A.; Gao, P.; Humphry-Baker, R.; Curchod, B. F. E.; Ashari-Astani, N.; Tavernelli, I.; Rothlisberger, U.; Nazeeruddin, M. K.; Grätzel, M. *Nat. Chem.* **2014**, *6*, 242−247. (c) Yella, A.; Mai, C.-L.; Zakeeruddine, S. M.; Chang, S.-N.; Hsieh, C.-H.; Yeh, C.-Y.; Grätzel, M. *Angew. Chem., Int. Ed.* **2014**, *53*, 2973−2977.

(3) (a) Burschka, J.; Pellet, N.; Moon, S.-J.; Humphry-Baker, R.; Gao, P.; Nazeeruddin, M. K.; Grätzel, M. *Nature* **2013**, *499*, 316−320. (b) Liu, M.; Johnston, M. B.; Snaith, H. J. *Nature* **2013**, *501*, 395−399. (c) Wojciechowski, K.; Saliba, M.; Leijtens, T.; Abate, A.; Snaith, H. J. *Energy Environ. Sci.* **2014**, *7*, 1142−1147. (d) Kim, H.-S.; Im, S. H.; Park, N.-G. *J. Phys. Chem. C* **2014**, *118*, 5615−5625. (e) Kazim, S.; Nazeeruddin, M. K.; Grätzel, M.; Ahmad, S. *Angew. Chem., Int. Ed.* **2014**, *53*, 2812−2824. (f) Pellet, N.; Gao, P.; Gregori, G.; Yang, T.-Y.; Nazeeruddin, M. K.; Maier, J.; Grätzel, M. *Angew. Chem., Int. Ed.* **2014**, *53*, 3151−3157.

(4) (a) Chen, B.-S.; Chen, K.; Hong, Y.-H.; Liu, W.-H.; Li, T.-H.; Lai, C.-H.; Chou, P.-T.; Chi, Y.; Lee, G.-H. *Chem. Commun.* **2009**, 5844−5846. (b) Chou, C.-C.; Wu, K.-L.; Chi, Y.; Hu, W.-P.; Yu, S. J.; Lee, G.-H.; Lin, C.-L.; Chou, P.-T. *Angew. Chem., Int. Ed.* **2011**, *50*, 2054−2058. (c) Wu, K.-L.; Li, C.-H.; Chi, Y.; Clifford, J. N.; Cabau, L.;

Palomares, E.; Cheng, Y.-M.; Pan, H.-A.; Chou, P.-T. *J. Am. Chem. Soc.* **2012**, *134*, 7488−7496. (d) Kinoshita, T.; Dy, J. T.; Uchida, S.; Kubo, T.; Segawa, H. *Nat. Photonics* **2013**, *7*, 535−539. (e) Numata, Y.; Singh, S. P.; Islam, A.; Iwamura, M.; Imai, A.; Nozaki, K.; Han, L. *Adv. Funct. Mater.* **2013**, *23*, 1817−1823.

(5) Nazeeruddin, M. K.; Pechy, P.; Renouard, T.; Zakeeruddin, S. M.; Humphyry-Baker, R.; Comte, P.; Liska, P.; Cevey, L.; Costa, E.; Shklover, V.; Spiccia, L.; Deacon, G. B.; Bignozzi, C. A. *J. Am. Chem. Soc.* **2001**, *123*, 1613−1624.

(6) (a) Wang, Z.-S.; Yamaguchi, T.; Sugihara, H.; Arakawa, H. *Langmuir* **2005**, *21*, 4272−4276. (b) Chiba, Y.; Islam, A.; Watanabe, Y.; Komiya, R.; Koide, N.; Han, L. *Jpn. J. Appl. Phys.* **2006**, *45*, L638−L640. (c) Ozawa, H.; Awa, M.; Ono, T.; Arakawa, H. *Chem. Asian J.* **2012**, *7*, 156−162. (d) Ozawa, H.; Okuyama, Y.; Arakawa, H. *Dalton Trans.* **2012**, *41*, 5137−5139.

(7) (a) Ogura, R.; Nakane, S.; Morooka, M.; Orihashi, M.; Suzuki, Y.; Noda, K. *Appl. Phys. Lett.* **2009**, *94*, 073308. (b) Han, L.; Islam, A.; Chen, H.; Malapaka, C.; Chiranjeevi, B.; Zhang, S.; Yang, X.; Yanagida, M. *Energy Environ. Sci.* **2012**, *5*, 6057−6060. (c) Ozawa, H.; Shimizu, R.; Arakawa, H. *RSC Adv.* **2012**, *2*, 3198−3200. (d) Ozawa, H.; Okuyama, Y.; Arakawa, H. *RSC Adv.* **2013**, *3*, 9175−9177. (e) Numata, Y.; Zhang, S.; Yang, X.; Han, L. *Chem. Lett.* **2013**, *42*, 1328−1335. (f) Zhang, S.; Islam, A.; Yang, X.; Qin, C.; Zhang, K.; Numata, Y.; Chen, H.; Han, L. *J. Mater. Chem. A* **2013**, *1*, 4812−4819. (g) Ozawa, H.; Okuyama, Y.; Arakawa, H. *ChemPhysChem* **2014**, *15*, 1201−1206.

(8) (a) Kim, H.-S.; Lee, C.-R.; Im, J.-H.; Lee, K.-B.; Moehl, T.; Marchioro, A.; Moon, S.-J.; Humphry-Baker, R.; Yum, J.-H.; Moser, J. E.; Grätzel, M.; Park, N.-G. *Sci. Rep.* **2012**, *2*, 591. (b) Im, J.-H.; Lee, C.-R.; Lee, J.-W.; Park, S.-W.; Park, N.-G. *Nanoscale* **2011**, *3*, 4088−4093.

(9) (a) Wang, P.; Klein, C.; Humphry-Baker, R.; Zakeeruddin, S. M.; Gräzel, M. *J. Am. Chem. Soc.* **2005**, *127*, 808−809. (b) Chen, C.-Y.; Wu, S.-J.; Wu, C.-G.; Chen, J.-G.; Ho, K.-C. *Angew. Chem., Int. Ed.* **2006**, *45*, 5822−5825. (c) Gao, F.; Wang, Y.; Zhang, J.; Shi, D.; Wang, M.; Humphry-Baker, R.; Wang, P.; Zakeeruddin, S. M.; Gräzel, M. *Chem. Commun.* **2008**, 2635−2637. (d) Chen, C.-Y.; Chen, J.-G.; Wu, S.-J.; Li, J.-Y.; Wu, C.-G.; Ho, K.-C. *Angew. Chem., Int. Ed.* **2008**, *47*, 7342−7345. (e) Li, J.-Y.; Chen, C.-Y.; Chen, J.-G.; Tan, C.-J.; Lee, K.-M.; Wu, S.-J.; Tung, Y.-L.; Tsai, H.-H.; Ho, K.-C.; Wu, C.-G. *J. Mater. Chem.* **2010**, *20*, 7158−7164. (f) Kim, J.-J.; Choi, H.; Paek, S.; Kim, C.; Lim, K.; Ju, M.-J.; Kang, H. S.; Kang, M.-S.; Ko, J. *Inorg. Chem.* **2011**, *50*, 11340−11347. (g) Bomben, P. G.; Gordon, T. J.; Scott, E.; Berlinguette, C. P. *Angew. Chem., Int. Ed.* **2011**, *50*, 10682−10685. (h) Bomben, P. G.; Borau-Garcia, J.; Berlinguette, C. P. *Chem. Commun.* **2012**, *48*, 5599−5601. (i) Yang, S.-H.; Wu, K.-L.; Chi, Y.; Cheng, Y.-M.; Chou, P.-T. *Angew. Chem., Int. Ed.* **2011**, *50*, 8270−8274. (j) Kimura, M.; Masuo, J.; Tohata, Y.; Obuchi, K.; Masaki, N.; Murakami, T. N.; Koumura, N.; Hara, K.; Fukui, A.; Yamanaka, R.; Mori, S. *Chem. Eur. J.* **2013**, *19*, 1028−1034. (k) Ozawa, H.; Kawaguchi, H.; Okuyama, Y.; Arakawa, H. *Chem. Lett.* **2011**, *40*, 658−660. (l) Ozawa, H.; Kawaguchi, H.; Okuyama, Y.; Arakawa, H. *Ambio* **2012**, *41*, 149−150. (m) El-Shafei, A.; Hussain, M.; Atiq, A.; Islam, A.; Han, L. *J. Mater. Chem.* **2012**, *22*, 24048−24056. (n) Hussain, M.; El-Shafei, A.; Islam, A.; Han, L. *Phys. Chem. Chem. Phys.* **2013**, *15*, 8401−8408. (o) El-Shafei, A.; Hussain, M.; Islam, A.; Han, L. *J. Mater. Chem. A* **2013**, *1*, 13679−13686. (p) Ozawa, H.; Yamamoto, Y.; Fukushima, K.; Yamashita, S.; Arakawa, H. *Chem. Lett.* **2013**, *42*, 897−899. (q) Ozawa, H.; Kawaguchi, H.; Okuyama, Y.; Arakawa, H. *Eur. J. Inorg. Chem.* **2013**, 5187−5195.

(10) (a) Ozawa, H.; Oura, S.; Shimizu, R.; Arakawa, H. *Chem. Lett.* **2012**, *41*, 1406−1408. (b) Ozawa, H.; Fukushima, K.; Sugiura, T.; Urayama, A.; Arakawa, H. *Dalton Trans.* **2014**, *43*, 13208−13218.

(11) García-Iglesias, M.; Yum, J.-H.; Humphry-Baker, R.; Zakeeruddin, S. M.; Péchy, P.; Vázquez, P.; Palomares, E.; Grätzel, M.; Nazeeruddin, M. K.; Torres, T. *Chem. Sci.* **2011**, *2*, 1145−1150.

(12) (a) Duffy, N. W.; Dobson, K. D.; Gordon, K. C.; Robinson, B. H.; McQuillan, A. J. *Phys. Chem. Lett.* **1997**, *266*, 451−455. (b) Finnie, K. S.; Bartlett, J. R.; Woolfrey, J. L. *Langmuir* **1998**, *14*, 2744−2749. (c) Vittadini, A.; Selloni, A.; Rotzinger, F. P.; Grätzel, M. *J. Phys. Chem., B* **2000**, *104*, 1300−1306. (d) Bauer, C.; Boschloo, G.; Mukhtar, E.; Hagfeldt, A. *J. Phys. Chem. B* **2002**, *106*, 12693−12704. (e) Nazeeruddin, M. K.; Humphyry-Baker, R.; Liska, P.; Grätzel, M. *J. Phys. Chem. B* **2003**, *107*, 8981−8987. (f) Klein, C.; Nazeeruddin, M. K.; Censo, D. D.; Liska, P.; Grätzel, M. *Inorg. Chem.* **2004**, *43*, 4216−4226. (g) Nazeeruddin, M. K.; Humphyry-Baker, R.; Officer, D. L.; Campbell, W. M.; Burrell, A. K.; Grätzel, M. *Langmuir* **2004**, *20*, 6514−6517.